Draft version October 13, 2021
Typeset using LaTeX twocolumn style in AASTeX63

Detecting Baryon Acoustic Oscillations with third generation gravitational wave observatories

Sumit Kumar,[1,2] Aditya Vijaykumar,[3] and Alexander H. Nitz[1,2]

[1] Max-Planck-Institut für Gravitationsphysik (Albert-Einstein-Institut), D-30167 Hannover, Germany
[2] Leibniz Universität Hannover, D-30167 Hannover, Germany
[3] International Centre for Theoretical Sciences, Tata Institute of Fundamental Research, Bangalore 560089, India

ABSTRACT

We explore the possibility of detecting Baryon Acoustic Oscillations (BAO) solely from gravitational wave observations of binary neutron star mergers with third generation (3G) gravitational wave (GW) detectors like Cosmic Explorer and the Einstein Telescope. These measurements would provide a new independent probe of cosmology. The detection of the BAO peak with current generation GW detectors (solely from GW observations) is not possible because i) unlike galaxies, the GW mergers are poorly localized and ii) there are not enough merger events to probe the BAO length scale. With the 3G GW detector network, it is possible to observe $\sim \mathcal{O}(1000)$ binary neutron star mergers per year localized well within one square degree in the sky for redshift $z \leq 0.3$. We show that 3G observatories will enable precision measurements of the BAO feature in the large-scale two-point correlation function; the effect of BAO can be independently detected at different reshifts, with a log-evidence ratio of $\sim$ 23, 17, or 3 favouring a model with a BAO peak at redshift of 0.2, 0.25, or 0.3, respectively, using a redshift bin corresponding to a shell of thickness $150h^{-1}$ Mpc.

Keywords: gravitational waves — binary neutron stars — baryon acoustic oscillations — third generation detectors

1. INTRODUCTION

The catalog of gravitational wave (GW) transients from compact binary mergers has grown considerably (Abbott et al. 2019, 2021b; Nitz et al. 2019, 2021; Venumadhav et al. 2020) since the first detection of gravitational waves from the merger of the binary black hole GW150914 (Abbott et al. 2016). This growing catalog of mergers has already revolutionized our understanding of the astrophysical rates and populations of compact objects, and has enabled precision tests of general relativity and cosmology (Abbott et al. 2021c,a). The sensitivity of the current ground-based GW detector network to compact binary mergers is expected to improve when the LIGO (Aasi et al. 2015), Virgo (Acernese et al. 2015) and KAGRA (Akutsu et al. 2020) detectors undergo upgrades (Abbott et al. 2018), and also with the construction of new detectors like LIGO-India (Saleem et al. 2021). Additionally, third generation (3G) detectors such as Einstein Telescope (ET) (Sathyaprakash et al. 2012) and Cosmic Explorer (CE) (Reitze et al. 2019a) will have an order-of-magnitude better strain sensitivity and will also be able to probe lower GW frequencies. It is also expected that they will localize most GW mergers within a few square degrees, while detecting hundreds of thousands of binary mergers each year (Mills et al. 2018). A number of precision tests of astrophysics and cosmology will be enabled as a result—for instance, studying the spatial distribution of a large number of well-localized sources, one can probe the large scale distribution of matter in the universe (Vijaykumar et al. 2020; Mukherjee et al. 2021a; Libanore et al. 2021; Mukherjee et al. 2021b). These probes using GW observations could confirm if the distribution of GW mergers indeed track the galaxy distribution, and can provide an independent probe to the features mostly attributed to galaxy or quasar population e.g. clustering bias (Kaiser 1984).

In this study, we investigate the possibility of probing another feature of the cosmological large scale structure—baryon acoustic oscillations—with third generation GW detectors. The layout of the paper is as follows: in Section 2 we give a brief overview of cosmological probes with GW observations, and motivate

Corresponding author: Sumit Kumar
sumit.kumar@aei.mpg.de

baryon acoustic oscillations as an independent probe of large scale structure. In Section 3, we describe the configurations of the 3G GW detector network used in this study. We describe our methodology to generate mock binary neutron star observations in Section 4, along with estimates of the measurability of the BAO feature in the correlation function. We end by summarizing our results and future directions in Section 5.

2. COSMOLOGY AND GRAVITATIONAL WAVES

Data from various cosmological surveys indicate that the evolution and current state of the Universe is best described by the standard model of cosmology, also referred to as the ΛCDM model (Riess et al. 1998). This model includes dark energy (described by the cosmological constant Λ in Einstein's equations) as the dominant component, along with dark matter (a pressureless fluid which interacts with standard model particles purely through gravitational forces), and baryonic matter (which includes directly observable matter such as galaxies and the intergalactic medium). Given a cosmological model and a set of parameters, one can derive the relation between the distance to an astronomical object, and the cosmological redshift z due to cosmic expansion. Conversely, independent measurements of the distances and z from observations can be turned into into measurements of the cosmological model parameters.

In the last few years, a 4.4σ discrepancy has been reported between the value of the Hubble parameter H_0 measured using early universe (Aghanim et al. 2020) and late universe (Riess et al. 2019) probes, hinting either at unknown systematics in the measurements, or at a "Hubble Tension" and possible deviation from the ΛCDM paradigm. The independent measurement of the Hubble parameter using GWs from compact binaries is ideally suited to provide more clarity in this regard. The characteristic luminosity of GW sources provide a direct measurement of the luminosity distance out to the sources (Schutz 1986). If the redshift of these sources can be measured using any other methods like the detection of an electromagnetic counterpart (Holz & Hughes 2005; Dalal et al. 2006; Nissanke et al. 2013) statistical identification of the host galaxy using a galaxy catalog (Del Pozzo 2012; Chen et al. 2018), a measurement of the tidal parameter (Messenger & Read 2012), or a physical scale in the mass distribution of sources (Farr et al. 2019), one can make a measurement of the Hubble parameter. It is expected that a measurement accuracy of $\sim 4.4\%$ can be reached with ~ 250 binary neutron star merger detections (Gray et al. 2020).

Another avenue of study in cosmology where GW observations show promise is their use as tracers to study the large-scale structure of the Universe. Similar to how galaxy surveys are used to probe large scale clustering, a population of GW sources can be used to probe the cosmological large scale structure by either the three-dimensional autocorrelation of the sources (Vijaykumar et al. 2020), or by cross-correlating the sources with other tracers of large-scale structure (Bera et al. 2020; Mukherjee et al. 2021a; Libanore et al. 2021; Mukherjee et al. 2021b). These allow for constraints to be put on the large-scale bias of gravitational wave events $b_{\rm GW}$, as well as the parameters of the standard ΛCDM model of cosmology.

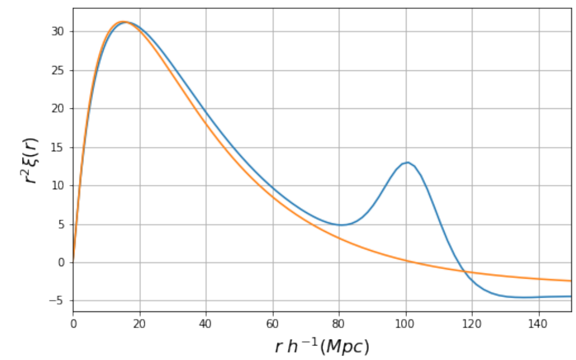

Figure 1. An example of two point correlation function $\xi(r)$ as a function of comoving distance r. Here we show two correlation functions: i) $\xi(r)$ showing a BAO feature at the scale of ~ 100 h^{-1}Mpc is calculated using transfer function prescribed by Eisenstein and Hu (Eisenstein & Hu 1998a), and ii) $\xi(r)$ without the BAO feature is calculated using BBKS (Bardeen et al. 1986) transfer function. We assume ΛCDM cosmological model parameters consistent with the Planck 2015 data (Ade et al. 2016). We multiply the two point correlation function $\xi(r)$ with r^2 on vertical axis for better visualization of BAO peak. The units on horizontal axis are h^{-1} Mpc where h is defined in terms of Hubble constant $H_0 = 100h$ km s^{-1} Mpc^{-1}

In this work, we ascertain the possibility of probing another feature in large-scale clustering of matter, namely baryon acoustic oscillations (BAO) (Sakharov 1966; Peebles & Yu 1970; Sunyaev & Zeldovich 1970; Eisenstein & Hu 1998b). BAO are imprints left by early-time sound waves in the Universe on the late-time distribution of matter. In the early Universe (at redshifts > 1089), high temperatures prevented the existence of bound atoms, and the primordial gas existed as ionized plasma. Free electrons in this plasma interacted with photons via Thomson scattering, thus coupling the baryons, electrons and photons into an effective fluid. The competing forces of electromagnetic radiation pressure and gravity in this fluid generated perturbations, thus setting up sound waves in the fluid.

Table 1. The specifications of each detector (location, noise curves, low frequency cutoff f_{low}) considered in this study. As the sites for 3G detectors are not yet finalized, we use the fiducial locations. The change in the final configuration should not significantly affect the localization results obtained this study. For CE detector, subscript (1, 2) represents (early, late) noise sensitivity curves and superscript (U, A) represents location of these detector (USA, Australia). These detectors configuration for CE and ET are taken from (Nitz & Dal Canton 2021)

Abbreviation	Observatory	$f_{\rm low}$	Noise Curve	Latitude	Longitude
C_1^U	Cosmic Explorer USA	5.2	CE1	40.8	-113.8
C_1^A	Cosmic Explorer Australia	5.2	CE1	-31.5	118.0
C_2^U	Cosmic Explorer USA	5.2	CE2	40.8	-113.8
C_2^A	Cosmic Explorer Australia	5.2	CE2	-31.5	118.0
E	Einstein Telescope	2	ET-D Design	43.6	10.5

During the epoch of recombination ($z \sim 1089$), the Universe cooled down enough for stable atoms to form—this thwarted the Thomson scattering, and destroyed the coupling. The photons then free-streamed and formed what we now know as the Cosmic Microwave Background (CMB), while the perturbations froze at a certain scale. As the Universe evolved and formed structures, this scale got imprinted on the distribution of halos and galaxies in the Universe at late times, appearing as a peak in the two point correlation function. For reviews on BAO, see (Bassett & Hlozek 2009; Weinberg et al. 2013).

The first confident signature of BAO from galaxy surveys came from the 3.4σ detection in the large-scale correlation function of luminous red galaxies (LRG) from Sloan Digital Sky Survey (SDSS) Data Release 3 (Eisenstein et al. 2005). These measurements have been confirmed by other samples like the 6-degree Field Galaxy Survey (Beutler et al. 2011), the WiggleZ Dark Energy Survey (Blake et al. 2011a,b), and most recently by the SDSS-IV extended Baryon Oscillation Spectroscopic Survey (eBOSS) (Alam et al. 2021; Bautista et al. 2020).

The BAO signature can be seen in the correlation function as a peak at comoving scale of $\sim$100 h^{-1} Mpc. In figure 1, we show the three dimensional correlation function $\xi(r)$ calculated using a transfer function fit provided by Eisenstein-Hu (Eisenstein & Hu 1998a) (with BAO feature) and by Bardeen et al (Bardeen et al. 1986) BBKS (without BAO feature). This signature can also be captured by two-point angular correlation function (2PACF) $w(\theta)$. Given a galaxy survey, one can estimate the correlation function using various estimators, most notably the Landy-Szalay estimator (Landy & Szalay 1993). For the localization volumes of typical binary mergers, the errors along the radial direction are larger compared to errors in angular direction when those errors are converted into comoving length scales. It is hence convenient to measure the 2PACF from GW merger events, provided that the radial uncertainties are not large enough to smear away information in the correlation function at the scales of interest. In general, one needs to take into account the smearing of the measured correlation function due to localization errors (Vijaykumar et al. 2020), and projection effects (Limber 1954) to track the effective shape of 2PACF $w(\theta)$.

3. THIRD GENERATION DETECTOR NETWORK

The proposed third generation (3G) detectors such as CE (Reitze et al. 2019b; Evans et al. 2021) and ET (Punturo et al. 2010) are expected to be operational sometime in next decade (2030s). CE is proposed to be built in two stages with upgrade consists of increasing design complexity and better sensitivity, known as CE1 and CE2 (Hall et al. 2020). ET is proposed to have good sensitivity at low frequency (Hild et al. 2011); we consider the design sensitivity $f_{\rm low}$ = 2Hz of ET for this study. The location of these detectors are not yet finalized but we use a fiducial location for these detectors: one CE in USA and the other CE in Australia which provides a long baseline. These fiducial detector locations are also used in previous works (Hall & Evans 2019; Nitz & Dal Canton 2021) We consider the location of ET to be in Europe. Table 1 lists the properties of the detectors we consider in this study. In this study, we focus on the localization capabilities of the 3G detector network only. Any 2G detector(s) added to the network would only further enhance the localization capabilities of the network. We consider following detector network configurations:
i) $C_1^U C_1^A E$: Two CE detectors (One in USA and other in Australia) and ET (In Europe), where the CE detectors have the early phase design sensitivity CE1, and
ii) $C_2^U C_2^A E$: Same as above, but the CE with second phase design sensitivity CE2.

Although we examine these specific configurations of the worldwide detector network, we do not expect other detector network configurations to change the distribution of localization errors of BNS events significantly as

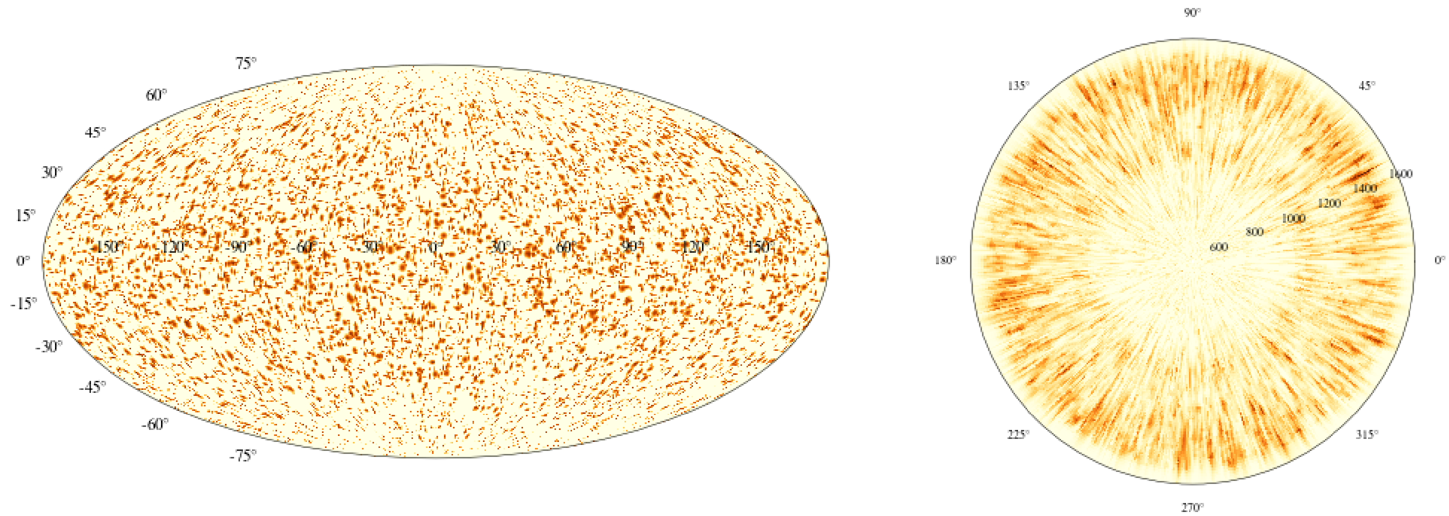

Figure 2. A realization of combined posterior field for the marginalized localization posterior from the simulation of of BNS events using 3G detector network. Left panel shows the marginalized posteriors for right ascension (RA) and declination (dec) angles. Right panel shows the marginalized posteriors on RA and comoving distance (along radial direction).

long as they include several next-generation observatories.

4. SIMULATIONS AND RESULTS

Next generation detectors will significantly improve the localization for both BNS and BBH mergers, and due to the higher intrinsic merger rates, we expect to get a much larger number of BNS events with highly precise localization volumes at low redshift ($z < 0.3$). Although we only consider BNS simulations in this study, our method can be readily generalized to BBHs.

We create many copies of the Universe containing BNS events observed with 3G detector networks. Each copy of the Universe is a realization of the observed BNS events with localization posterior and we call it BNS catalog. To create such BNS catalog, we create a realization of universe containing large number of galaxies (fiducial galaxy catalog), a (randomly selected) small fraction of which can act as the host galaxies to BNS events. These galaxies need to be distributed spatially in such a way that underlying correlation function contains the BAO peak as shown in figure 1. To create these BNS catalogs, we need i)the density of BNS events detectable with the 3G detector network, and ii) the localization distribution of BNS events.

4.1. *BNS population distribution*

To generate a realistic population of BNS, we use the Madau-Dickinson star formation rate (SFR) $\psi(z)$ (Madau & Dickinson 2014),

$$\psi(z) = 0.015 \frac{(1+z)^{2.7}}{1 + [(1+z)/2.9]^{5.6}} \ \mathrm{M_{\odot} yr^{-1} Mpc^{-3}} \quad (1)$$

We assume that the local formation rate of the BNS is proportional to the SFR. To get the merger rate, the SFR is corrected with a delay time distribution $p(t_D) \sim 1/t_D \sim 1/(t - t_f)$ where t_f is the formation time of the binary.

$$\Psi(z) = \int_{z_f}^{z} \psi(z') \ P(t(z') - t_f) \, \mathrm{d}z' \quad (2)$$

This choice of the delay time distribution is motivated by classical isolated binary evolution models (O'Shaughnessy et al. 2010; Dominik et al. 2012). We normalize 2 such that $\Psi(z = 0)$ gives us the local merger rate of 320 $\mathrm{yr^{-1} Gpc^{-3}}$, the median estimated merger rate of BNS mergers from GWTC-2 (Abbott et al. 2021d). In the detector frame, the number density of of BNS mergers dN/dz is related to source frame merger rate $\Psi(z)$ by following relation,

$$\frac{dN}{dz} = \frac{dV_c}{dz} \frac{\Psi(z)}{1+z} \quad (3)$$

Where V_c is the comoving volume. We integrate 3 in a given redshift bin and estimate the total number of BNS mergers $\Delta\mathcal{N}(z)$ expected in that redshift bin from 3G detectors. The results we thus obtain are consistent with (Mills et al. 2018).

4.2. *Parameter estimation*

To estimate the localization posterior for each simulated BNS source, we make use Bayesian parameter estimation using the publicly available code PyCBC Inference (Biwer et al. 2019). We distribute non-spinnning BNS sources assuming the source frame component

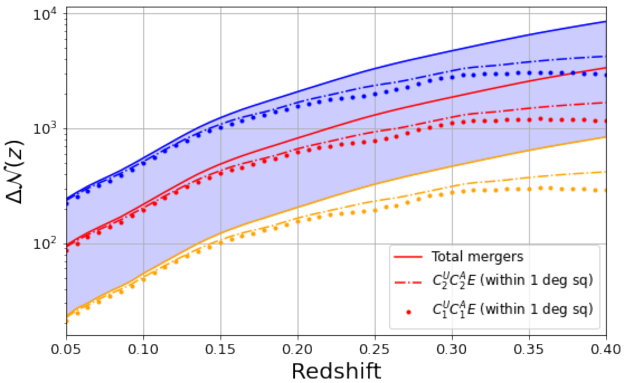

Figure 3. The number of BNS mergers in a shell of thickness 150 h^{-1} Mpc as a function of redshift. Solid lines represents total number of mergers, dotted-dashed and dashed lines represent the BNS mergers with sky localization within 1 square degree in that shell for two detector network (See text for explanation).

masses to be equal to 1.4 $M_\odot$. Since the mass distribution of neutron stars is narrow, we do not expect the results of the study to differ significantly with any other mass distributions for BNS sources. We assume that the sources are distributed isotropically in sky and orientation for inclination angle, and uniformly in comoving distance. The redshift (or distance) distribution can be obtained by rescaling base population to desired rate as a function of redshift such as in 3. We use heterodyne likelihood model (Cornish 2010; Finstad & Brown 2020; Zackay et al. 2018) to estimate the likelihood function. We choose following parameters to vary in parameter estimation: chirp mass: $\mathcal{M}$, mass ratio: q, $(q > 1)$, inclination angle, luminosity distance: D_L, Right Ascension: RA, declination: dec, polarization angle, merger time:t_c. We use uniform priors on $\mathcal{M}$ (detector frame), q, and t_c and isotropic priors for RA, dec, inclination angle, and polarization. For distance, we choose a prior uniform in comoving volume. We use the TaylorF2 waveform model (Blanchet et al. 1995; Faye et al. 2012) to simulate our signal in gaussian noise, and for signal recovery while estimating source parameters. TaylorF2 excludes the merger from the analysis but we still recover significant signal to noise ratio (SNR) due to long signal length and enhanced low frequency sensitivity of 3G detectors. Due to the significantly low frequency cutoff of ET ($f_{low} \sim 2Hz$), the length of the signal is very long and hence we take earth rotation effects into account. We sample the signal at 1024 Hz, and introduce a high frequency cut-off of 512 Hz for evaluation of the likelihood function in order to reduce computational costs. Ideally, the high-frequency cutoff should be much larger, but this does not cause a significant loss in SNR compared to the full signal, and we are still able to get highly localized posteriors for the redshift range we are interested in. To sample over the parameters, we use a sampler based on a dynamical nested sampling algorithm (Higson et al. 2018; Skilling 2006) implemented in software package DYNESTY (Speagle 2020). We let the sampler run until most of the prior volume is spanned by 'live points' and the estimated remaining log-evidence ($dlogZ$) is equal to a small value of 0.1.

4.3. *Methodology*

For the purposes of this study, we assume that BNS events are hosted in galaxies and hence they trace the underlying galaxy distribution. To create a realization of BNS events that trace the galaxy distribution, we first choose a shell centred around the redshift we are interested in, and generate an underlying fiducial galaxy catalog. We then randomly select the galaxies which can serve as set of host galaxies to BNS events and place the localization posteriors on top of these selected BNS events. The density of BNS event selected depends on the total number of mergers expected in the shell (which are localized within one degree square) and the localization posteriors are chosen from the parameter estimation simulations obtained from the base population in that redshift bin.

To generate the fiducial galaxy catalogs, we use publicly available code lognormal_galaxies (Agrawal et al. 2017).

The input power spectrum is calculated using the Eisenstein and Hu transfer function (Eisenstein & Hu 1998b) which contains the BAO peak. We assume standard ΛCDM cosmology with parameters consistent with Planck results (Ade et al. 2016). After construction of the galaxy catalog, we randomly select galaxies as host to the BNS merger events. Once the host galaxies are identified, we simulate a BNS source at that location and estimate the inferred posterior distribution from gravitational-wave observation. In figure 2 we show a realization of one such BNS catalog with marginalised posteriors for localization parameters. Each BNS catalog consists of N posterior samples combined to give posterior field $\mathcal{P} = \sum_{i=1}^{N} \mathcal{P}_i(RA, dec, D_C)$, where $\mathcal{P}_i$ is individual localization posterior for RA, dec, and comoving distance: D_c.

Once we have a BNS catalog at given redshift, to extract the BAO peak, we focus on a shell of thickness $\approx$ 150 h^{-1} Mpc at redshifts $z = \{0.2, 0.25, 0.3\}$. We use the following algorithm for extracting BAO peak:

- For a given redshift, choose a shell of thickness $\sim$ 150 h^{-1} Mpc in comoving volume. To avoid the autocorrelation of points from the same poste-

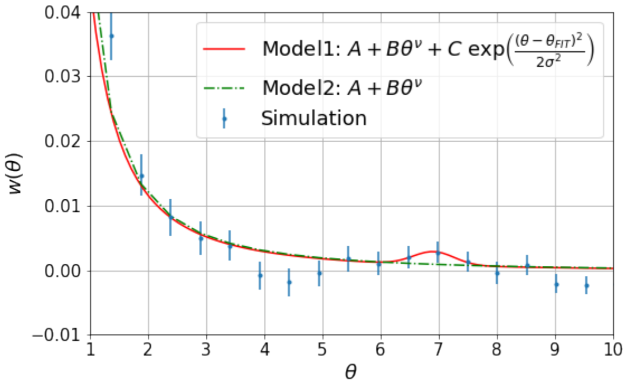

Figure 4. Angular two point correlation function recovery is shown here for a realization at the redshift of $z = 0.3$. We also show the fit to the data using the model described in the text. Input value for θ_{BAO} for $z = 0.3$ is 6.9 degrees. We estimate the difference in log evidence for both the models $ln\frac{Z1}{Z2} = 2.59$ indicating that model with BAO peak is favoured compared to model without BAO peak.

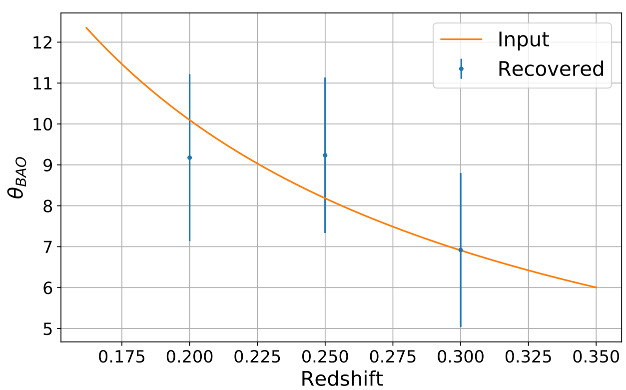

Figure 5. The recovery of BAO scale at different redshifts from a shell of thickness 150 h^{-1} Mpc taken around the given redshift. The solid continuous line shows the angular BAO scale as a function of redshift. We assume flat ΛCDM model with best fit parameters set to Planck 2015 results. The errors on the recovered BAO scale are estimated from averaging over 1000 catalogs to account for cosmic variance as well as statistical errors due to selecting host galaxies for BNS merger events from large galaxy catalogs. We estimate the difference in the log evidence for fit function for two models (with BAO against without BAO). For all the redshifts, the model with BAO peak is favoured (see text).

rior, randomly select one point from each posterior which lies within the chosen shell.

- Use the selected points to calculate 2PACF using the Landy-Szalay estimator *ie.*,

$$w_i(\theta) = \frac{DD_i(\theta) - 2DR_i(\theta) + RR_i(\theta)}{RR_i(\theta)}\ , \qquad (4)$$

where $DD_i(\theta)$ is the number of pairs of data points in the bin separated by angle θ, $RR_i(\theta)$ is the number of point-pairs in an equal-sized random catalog separated by θ, and $DR_i(\theta)$ is the number of data-random pairs separated by θ. We use the publicly available code Corrfunc (Sinha & Garrison 2019, 2020) to calculate the correlation function. To minimize the projection effects in the shell, we divide shell of 150 h^{-1} Mpc into smaller sub-shell of 60 h^{-1} Mpc with sliding window of 30 h^{-1} Mpc and take the average.

- Repeat the above procedure for different realizations of posterior field (by randomly selecting a point from each posterior) and estimate the average 2PACF $w(\theta) = \frac{1}{n}\sum_{i=1}^{n} w_i(\theta)$. For this study, we chose $n = 100$ for each sub-shell of 60 h^{-1} Mpc.

- Once we have recover $w(\theta)$, we model the 2PACF following Sanchez et al. (2011) as,

$$w(\theta) = A + B\theta^\nu + C\exp\left[-\frac{(\theta-\theta_{FIT})^2}{2\sigma_{FIT}^2}\right] \qquad (5)$$

This model has six parameters to fit the data: {A, B, C, ν, θ_{FIT}, σ_{FIT}}. The first two terms in the model gives the power law to fit the broad shape of the correlation function and the last term models the BAO peak as a Gaussian with location of peak as θ_{FIT} and width of the peak as σ_{FIT} along with amplitude C. To fit a model without BAO peak, we drop the last term in 5 and fit for remaining three parameters.

- To account for systematic and statistical errors, we generate 50 galaxy catalogs for each redshift corresponding to different seed for underlying density field. We then take 20 realizations from each galaxy catalog to account for statistical fluctuation in choosing the set of host galaxies. In this way we account for errors due to cosmic variance, errors arising from the sampling bias due to the selection of the host galaxies, and errors due to localization posteriors.

We do not correct the recovered 2PACF $w(\theta)$ for i) smearing effects due to localization errors, and ii) projection effects in a shell. This is justified because we do not track the exact shape of 2PACF. Rather, we are interested in the location of BAO peak in the 2PACF. As long as these effects do not destroy the BAO peak in the correlation function, we should be able to recover it. The recovery of BAO peak with BNS merger events is also a statistical effect: one can confuse a statistical

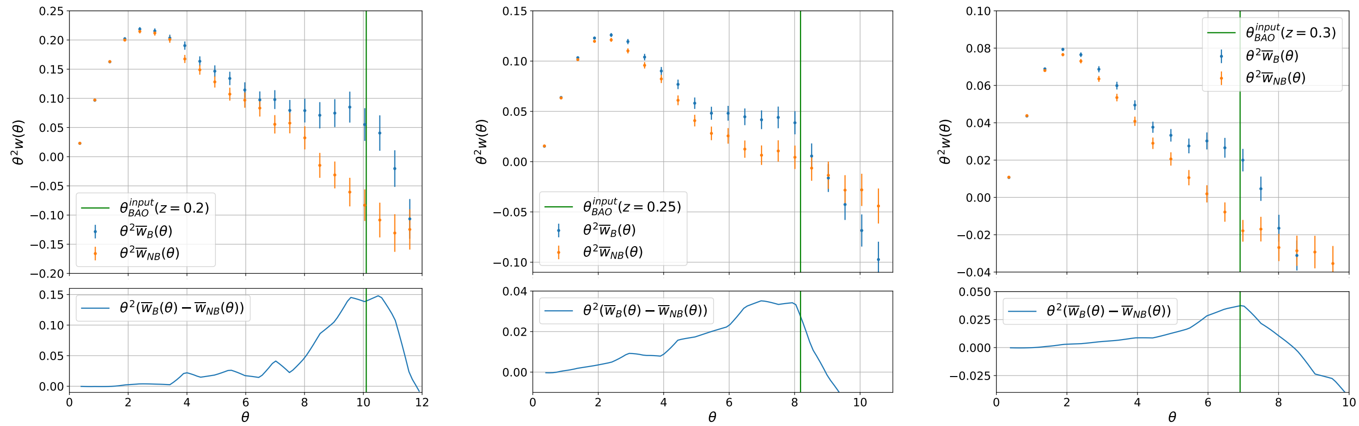

Figure 6. The average of the angular two point function for all the BNS catalogues for each redshift bin is plotted. $\overline{w}_B(\theta)$ represents average for all the catalogs which contain BAO peak and $\overline{w}_{NB}(\theta)$ is the same for the catalogs which do not contain BAO peak. In the upper panels, we show the 2PACF for both set of catalogs. The solid vertical line shows the input angular BAO scale at the given redshift. In the lower panel, we show the difference in the average correlation functions obtained from both set of catalogs. The statistical significance of of detection of a BAO peak can be estimated by comparing the recovered correlation function against the average for respective bins.

bump in correlation function with BAO peak. In order to be confidently recover the BAO peak, one must consider recovering BAO peak in various redshift bins.

4.4. *Results*

In figure 4, we show the recovery of the BAO peak in one realization of BNS merger events at the redshift $z = 0.3$. We estimate the input angular BAO scale at given redshift z using the relation $\theta_{BAO} = r_s/((1+z)D_A(z))$ where r_s is the BAO scale in terms of comoving distance and $D_A(z)$ is the angular diameter distance to given redshift. For this BNS catalog, we fit the models with and without BAO peak using DYNESTY (Speagle 2020) software package. We estimate the Bayesian evidence $\mathcal{Z}$ for both the models and compare them. The model with higher value (> 2.5) of $\mathcal{Z}$ is statistically preferred (Jeffreys 1998). The difference in log evidence between two models turns out to be $\ln(\mathcal{Z}_1/\mathcal{Z}_2) = 2.59$ indicating that model with BAO peak is favoured compared to model without BAO peak.

In figure 5 we show the the recovery of the BAO peak at different redshift bins. We estimate the Bayesian evidence for both models in these redshift bins. The $\ln(\mathcal{Z}_1/\mathcal{Z}_2)$ for these redshift bins is given by $23.29(z = 0.2)$, $16.73(z = 0.25)$, and $2.59(z = 0.3)$ again indicating that model with BAO peak is favoured. We show that with 7-10 years of observation, enough BNS merger events can be accumulated to recover the BAO peak within statistical errors.

To check the robustness of the method, we also generate ~ 1000 BNS catalogs from the corresponding galaxy catalogs which do not contain BAO peak. We use BBKS transfer function (Bardeen et al. 1986) to calculate input correlation function to generate such catalogs. We then estimate the average 2PACF $w(\theta)$ across all catalogs in respective catagories (with BAO peak and without BAO peak). In figure 6, we show that the average of 2PACF estimated from all the BNS mereger catalogs in two catagories: i) ones containing a BAO peak and ii) ones that do not a BAO peak. It can be seen that, statistically, we recover the BAO peak at the injected value. In these simulations, we find that the redshift window between $z \in [0.2, 0.3]$ is best suited for our study because we get a large number of BNS events with desired localization accuracy. Beyond $z > 0.3$, although we do get enough number of BNS events localized with a degree square, the localization errors along the radial direction start to dominate and become large enough to destroy the angular correlations as well. Since the BAO feature is very weak and is hard to detect, to account for statistical fluctuations, it is preferable to recover BAO feature in 2PACF in a sliding window of given shell thickness in the ideal redshift range described above.

These measurements in gravitational wave catalogs, apart from being independent probes of the BAO scale, provide the opportunity to constrain cosmological parameters by using the BAO scale as a standard ruler. At the low redshifts of interest to this study, r_s is a direct measure of the Hubble parameter H_0. Using the r_s and $\Omega_m h^2$ (where $h = H_0/100$) derived from CMB experiments in conjuction with the measurements from GW data, one can measure the value of Ω_m (Eisenstein et al. 1998). Alternatively, the measurements of the BAO scale θ_{BAO} at different redshifts can be used to measure r_s (Carvalho et al. 2016).

Although we use a GW detector network consisting only of 3G detectors, it is also possible that many current ground based detectors will still be in operation (with future upgrades). This scenario will only improve the localization of sources and hence a hybrid network consisting of 3G detectors such as CE, ET and 2G detectors such as LIGO, Virgo, KAGRA will greatly improve the localization of the GW sources.

In this study, we assumed that the network of detectors will have same sensitivity for all sky positions. Depending on the given network configuration and antenna pattern, we might get varying sensitivity for different parts of sky. Although for 3G detectors, we expect this effect to be small but one natural extension of this work is to include such effects. In future, we intend to extend this work to include smearing effects due to posteriors (Vijaykumar et al. 2020), projection effects due to shell thickness (Limber 1954), and more previous generation detectors along with 3G detector networks. The conclusions of the current work also rely on the range of estimated merger rates of BNS events (Abbott et al. 2021b). Future increase (decrease) in the estimation of merger rates would mean less (more) time will be required to accumulate enough BNS merger events.

5. SUMMARY

We have explored the possibility of detecting BAO scale using GW merger events in the 3G detector network. Probing the details of large scale structures (such as BAO scale) with GW observations is a challenging task because of poor localization of the GW sources and low number density of detected events. We find that with 3G detector network consisting of two CE (USA and Australia) and one ET (Europe), we can accumulate a large number ($\mathcal{O}(10000)$) of very well localized (within 1 square degree) BNS events upto the redshift ($z < 0.3$) in 7-10 years of observing time. This opens up the possibility to probe the BAO scale solely by GW observations and hence provide an independent probe to BAO. With the 3G detector network considered in this study, we find that the redshift range of 0.2-0.3 is best suited for recovery of BAO peak assuming that the GW merger population does track the galaxy distribution. The new probe for BAO might not only enable us to complement the observations from other surveys, it may provide opportunity to peek into the distribution of BNS with relation to galaxies and provide independent constraints on cosmological parameters. This study broadens the horizon of science goals which can be achieved by 3G detectors and emphasizes the need for 3G detector network for the future.

ACKNOWLEDGMENTS

We acknowledge the Max Planck Gesellschaft. We thank the computing team from AEI Hannover for their significant technical support. Authors thank Ajith Parameswaran, Tirthankar Roy Choudhury, Bruce Allen, and Badri Krishnan for useful discussions and valuable comments. AV would also like to thank members of the Astrophysical Relativity group at ICTS for feedback. SK would like to thank Xisco Jiménez Forteza for useful comments. AV's research is supported by the Department of Atomic Energy, Government of India, under Project No. RTI4001.

REFERENCES

Aasi, J., et al. 2015, Class. Quant. Grav., 32, 074001, doi: 10.1088/0264-9381/32/7/074001

Abbott, B., Abbott, R., Abbott, T., et al. 2016, Physical Review D, 93, doi: 10.1103/physrevd.93.122003

Abbott, B. P., et al. 2018, Living Rev. Rel., 21, 3, doi: 10.1007/s41114-020-00026-9

—. 2019, Phys. Rev. X, 9, 031040, doi: 10.1103/PhysRevX.9.031040

—. 2021a, Astrophys. J., 909, 218, doi: 10.3847/1538-4357/abdcb7

Abbott, R., et al. 2021b, Phys. Rev. X, 11, 021053, doi: 10.1103/PhysRevX.11.021053

—. 2021c, Phys. Rev. D, 103, 122002, doi: 10.1103/PhysRevD.103.122002

—. 2021d, Astrophys. J. Lett., 913, L7, doi: 10.3847/2041-8213/abe949

Acernese, F., et al. 2015, Class. Quant. Grav., 32, 024001, doi: 10.1088/0264-9381/32/2/024001

Ade, P. A. R., et al. 2016, Astron. Astrophys., 594, A13, doi: 10.1051/0004-6361/201525830

Aghanim, N., et al. 2020, Astron. Astrophys., 641, A6, doi: 10.1051/0004-6361/201833910

Agrawal, A., Makiya, R., Chiang, C.-T., et al. 2017, Journal of Cosmology and Astroparticle Physics, 2017, 003003, doi: 10.1088/1475-7516/2017/10/003

Akutsu, T., et al. 2020. https://arxiv.org/abs/2005.05574

Alam, S., et al. 2021, Phys. Rev. D, 103, 083533, doi: 10.1103/PhysRevD.103.083533

Bardeen, J. M., Bond, J. R., Kaiser, N., & Szalay, A. S. 1986, ApJ, 304, 15, doi: 10.1086/164143

Bassett, B. A., & Hlozek, R. 2009. https://arxiv.org/abs/0910.5224

Bautista, J. E., et al. 2020, Mon. Not. Roy. Astron. Soc., 500, 736, doi: 10.1093/mnras/staa2800
Bera, S., Rana, D., More, S., & Bose, S. 2020, Astrophys. J., 902, 79, doi: 10.3847/1538-4357/abb4e0
Beutler, F., Blake, C., Colless, M., et al. 2011, Mon. Not. Roy. Astron. Soc., 416, 3017, doi: 10.1111/j.1365-2966.2011.19250.x
Biwer, C. M., Capano, C. D., De, S., et al. 2019, Publ. Astron. Soc. Pac., 131, 024503, doi: 10.1088/1538-3873/aaef0b
Blake, C., et al. 2011a, Mon. Not. Roy. Astron. Soc., 418, 1707, doi: 10.1111/j.1365-2966.2011.19592.x
—. 2011b, Mon. Not. Roy. Astron. Soc., 415, 2892, doi: 10.1111/j.1365-2966.2011.19077.x
Blanchet, L., Damour, T., Iyer, B. R., Will, C. M., & Wiseman, A. G. 1995, Phys. Rev. Lett., 74, 3515, doi: 10.1103/PhysRevLett.74.3515
Carvalho, G. C., Bernui, A., Benetti, M., Carvalho, J. C., & Alcaniz, J. S. 2016, Phys. Rev. D, 93, 023530, doi: 10.1103/PhysRevD.93.023530
Chen, H.-Y., Fishbach, M., & Holz, D. E. 2018, Nature, 562, 545, doi: 10.1038/s41586-018-0606-0
Cornish, N. J. 2010. https://arxiv.org/abs/1007.4820
Dalal, N., Holz, D. E., Hughes, S. A., & Jain, B. 2006, Phys. Rev. D, 74, 063006, doi: 10.1103/PhysRevD.74.063006
Del Pozzo, W. 2012, Phys. Rev. D, 86, 043011, doi: 10.1103/PhysRevD.86.043011
Dominik, M., Belczynski, K., Fryer, C., et al. 2012, Astrophys. J., 759, 52, doi: 10.1088/0004-637X/759/1/52
Eisenstein, D. J., & Hu, W. 1998a, The Astrophysical Journal, 496, 605614, doi: 10.1086/305424
—. 1998b, Astrophys. J., 496, 605, doi: 10.1086/305424
Eisenstein, D. J., Hu, W., & Tegmark, M. 1998, Astrophys. J. Lett., 504, L57, doi: 10.1086/311582
Eisenstein, D. J., et al. 2005, Astrophys. J., 633, 560, doi: 10.1086/466512
Evans, M., Adhikari, R. X., Afle, C., et al. 2021, arXiv e-prints, arXiv:2109.09882. https://arxiv.org/abs/2109.09882
Farr, W. M., Fishbach, M., Ye, J., & Holz, D. 2019, Astrophys. J. Lett., 883, L42, doi: 10.3847/2041-8213/ab4284
Faye, G., Marsat, S., Blanchet, L., & Iyer, B. R. 2012, Class. Quant. Grav., 29, 175004, doi: 10.1088/0264-9381/29/17/175004
Finstad, D., & Brown, D. A. 2020, Astrophys. J. Lett., 905, L9, doi: 10.3847/2041-8213/abca9e
Gray, R., et al. 2020, Phys. Rev. D, 101, 122001, doi: 10.1103/PhysRevD.101.122001
Hall, E. D., & Evans, M. 2019, Classical and Quantum Gravity, 36, 225002, doi: 10.1088/1361-6382/ab41d6
Hall, E. D., et al. 2020. https://arxiv.org/abs/2012.03608
Higson, E., Handley, W., Hobson, M., & Lasenby, A. 2018, Statistics and Computing, 29, 891913, doi: 10.1007/s11222-018-9844-0
Hild, S., et al. 2011, Class. Quant. Grav., 28, 094013, doi: 10.1088/0264-9381/28/9/094013
Holz, D. E., & Hughes, S. A. 2005, Astrophys. J., 629, 15, doi: 10.1086/431341
Jeffreys, H. 1998, The Theory of Probability, Oxford Classic Texts in the Physical Sciences (OUP Oxford). https://books.google.de/books?id=vh9Act9rtzQC
Kaiser, N. 1984, Astrophys. J. Lett., 284, L9, doi: 10.1086/184341
Landy, S. D., & Szalay, A. S. 1993, Astrophys. J., 412, 64, doi: 10.1086/172900
Libanore, S., Artale, M. C., Karagiannis, D., et al. 2021, JCAP, 02, 035, doi: 10.1088/1475-7516/2021/02/035
Limber, D. N. 1954, Astrophys. J., 119, 655, doi: 10.1086/145870
Madau, P., & Dickinson, M. 2014, Ann. Rev. Astron. Astrophys., 52, 415, doi: 10.1146/annurev-astro-081811-125615
Messenger, C., & Read, J. 2012, Phys. Rev. Lett., 108, 091101, doi: 10.1103/PhysRevLett.108.091101
Mills, C., Tiwari, V., & Fairhurst, S. 2018, Phys. Rev., D97, 104064, doi: 10.1103/PhysRevD.97.104064
Mukherjee, S., Wandelt, B. D., Nissanke, S. M., & Silvestri, A. 2021a, Phys. Rev. D, 103, 043520, doi: 10.1103/PhysRevD.103.043520
Mukherjee, S., Wandelt, B. D., & Silk, J. 2021b, Mon. Not. Roy. Astron. Soc., 502, 1136, doi: 10.1093/mnras/stab001
Nissanke, S., Holz, D. E., Dalal, N., et al. 2013. https://arxiv.org/abs/1307.2638
Nitz, A. H., Capano, C. D., Kumar, S., et al. 2021. https://arxiv.org/abs/2105.09151
Nitz, A. H., & Dal Canton, T. 2021, The Astrophysical Journal Letters, 917, L27, doi: 10.3847/2041-8213/ac1a75
Nitz, A. H., Dent, T., Davies, G. S., et al. 2019, Astrophys. J., 891, 123, doi: 10.3847/1538-4357/ab733f
O'Shaughnessy, R., Kalogera, V., & Belczynski, K. 2010, Astrophys. J., 716, 615, doi: 10.1088/0004-637X/716/1/615
Peebles, P. J. E., & Yu, J. T. 1970, Astrophys. J., 162, 815, doi: 10.1086/150713
Punturo, M., Abernathy, M., Acernese, F., et al. 2010, Classical and Quantum Gravity, 27, 194002, doi: 10.1088/0264-9381/27/19/194002

Reitze, D., et al. 2019a, Bull. Am. Astron. Soc., 51, 035. https://arxiv.org/abs/1907.04833
—. 2019b, Bull. Am. Astron. Soc., 51, 035. https://arxiv.org/abs/1907.04833
Riess, A. G., Casertano, S., Yuan, W., Macri, L. M., & Scolnic, D. 2019, Astrophys. J., 876, 85, doi: 10.3847/1538-4357/ab1422
Riess, A. G., et al. 1998, Astron. J., 116, 1009, doi: 10.1086/300499
Sakharov, A. D. 1966, Soviet Journal of Experimental and Theoretical Physics, 22, 241
Saleem, M., et al. 2021. https://arxiv.org/abs/2105.01716
Sanchez, E., Carnero, A., Garcia-Bellido, J., et al. 2011, Mon. Not. Roy. Astron. Soc., 411, 277, doi: 10.1111/j.1365-2966.2010.17679.x
Sathyaprakash, B., et al. 2012, Class. Quant. Grav., 29, 124013, doi: 10.1088/0264-9381/29/12/124013
Schutz, B. F. 1986, Nature, 323, 310, doi: 10.1038/323310a0
Sinha, M., & Garrison, L. H. 2019, in Communications in Computer and Information Science: Proceedings of the 'Software Challenges to Exascale Computing' Second Workshop, SCEC 2018, Delhi, India, December 13-14 2018, Vol. 964, pp. 3-20, doi: 10.1007/978-981-13-7729-7_1
Sinha, M., & Garrison, L. H. 2020, Mon. Not. Roy. Astron. Soc., 491, 3022, doi: 10.1093/mnras/stz3157
Skilling, J. 2006, Bayesian Analysis, 1, 833 , doi: 10.1214/06-BA127
Speagle, J. S. 2020, Monthly Notices of the Royal Astronomical Society, 493, 3132, doi: 10.1093/mnras/staa278
Sunyaev, R. A., & Zeldovich, Y. B. 1970, Astrophys. Space Sci., 7, 3
Venumadhav, T., Zackay, B., Roulet, J., Dai, L., & Zaldarriaga, M. 2020, Phys. Rev. D, 101, 083030, doi: 10.1103/PhysRevD.101.083030
Vijaykumar, A., Saketh, M. V. S., Kumar, S., Ajith, P., & Choudhury, T. R. 2020. https://arxiv.org/abs/2005.01111
Weinberg, D. H., Mortonson, M. J., Eisenstein, D. J., et al. 2013, Phys. Rept., 530, 87, doi: 10.1016/j.physrep.2013.05.001
Zackay, B., Dai, L., & Venumadhav, T. 2018. https://arxiv.org/abs/1806.08792